Electronic Supplementary Material (ESI) for Dalton Transactions.
This journal is © The Royal Society of Chemistry 2020

***Hemilabile Manganese-Phenol Complex and its Coordination Induced O–H Bond Weakening***

Karthika J. Kadassery,[†] Matthew R. Crawley,[†] Samantha N. MacMillan,[§] David C. Lacy*[†]

† Department of Chemistry, University at Buffalo, State University of New York, Buffalo, New York 14260, United States
§ Department of Chemistry and Chemical Biology, Cornell University, Ithaca, New York 14853, United States

*Corresponding Author
E-mail: DCLacy@buffalo.edu

**Contents** **Page**

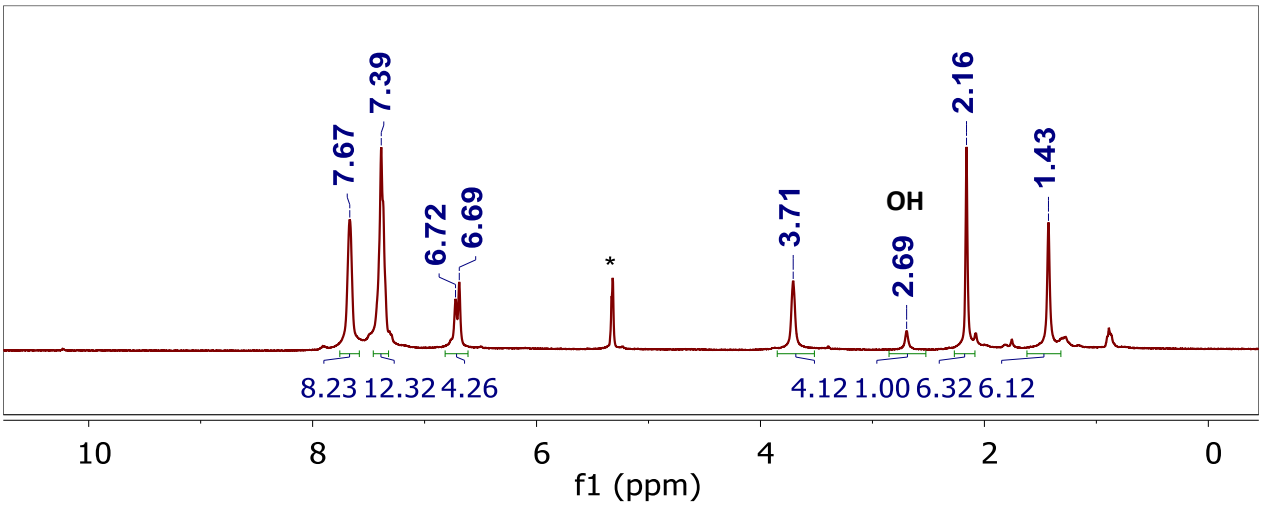


**Figure S1a:** $^{1}$H-NMR spectrum of $^{H}$**1** in $d_2$-DCM*.

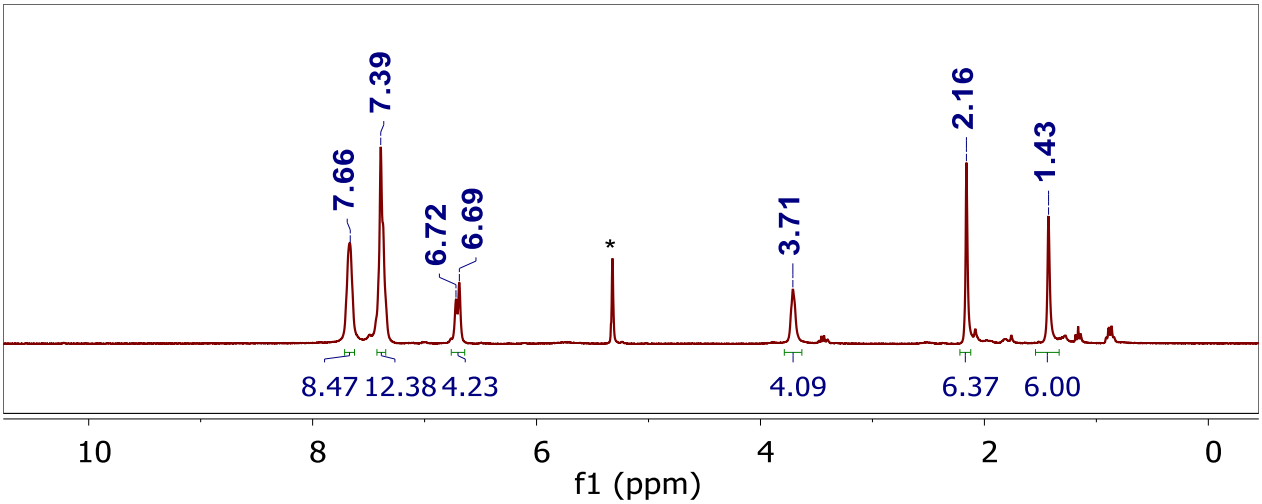


**Figure S1b:** $^{1}$H-NMR spectrum of $d_1$-$^{H}$**1** in $d_2$-DCM*.

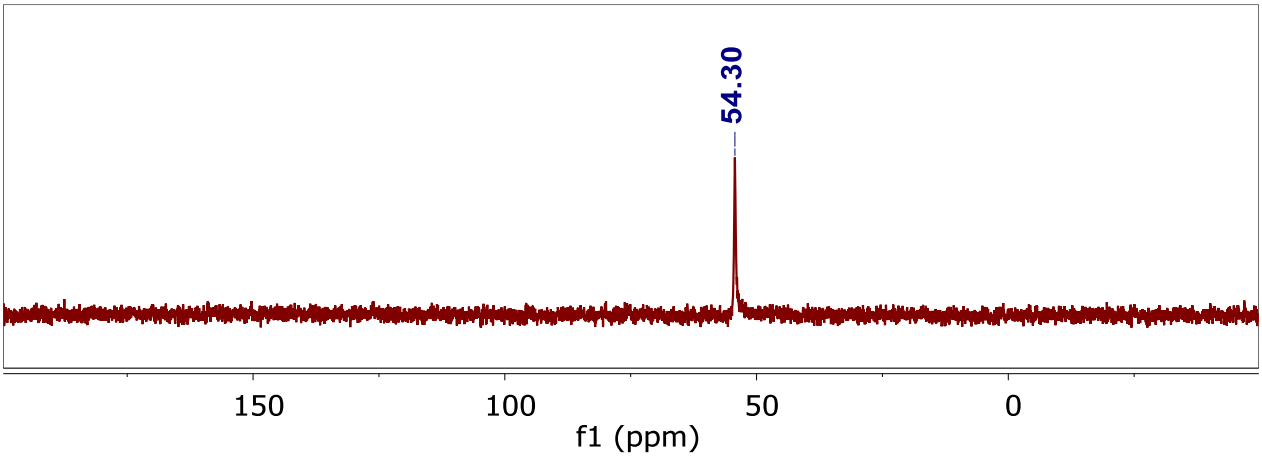


**Figure S2a:** $^{31}$P{$^{1}$H}-NMR spectrum of $^{H}$**1** in $d_2$-DCM.

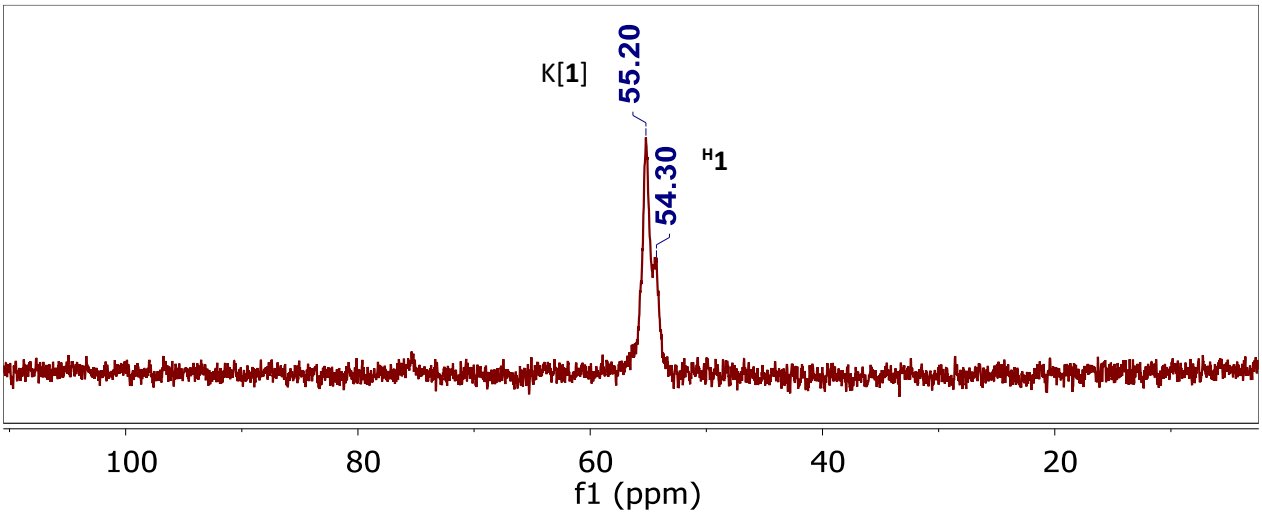


**Figure S2b:** $^{31}P\{^{1}H\}$-NMR spectrum of a mixture of K[**1**] and $^{H}$**1** in DCM.

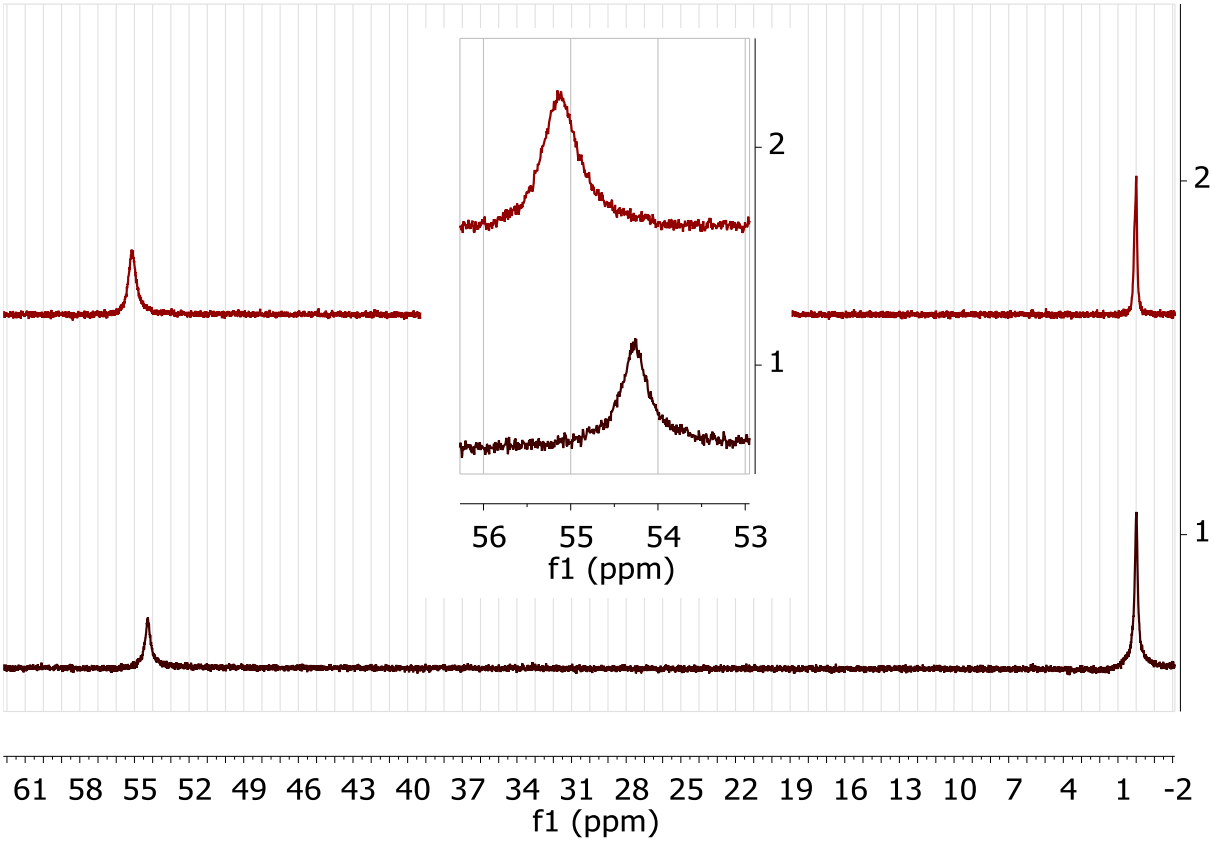


**Figure S2c:** $^{31}P\{^{1}H\}$-NMR spectra of (1) $^{H}$**1** and (2) K[**1**] in DCM.

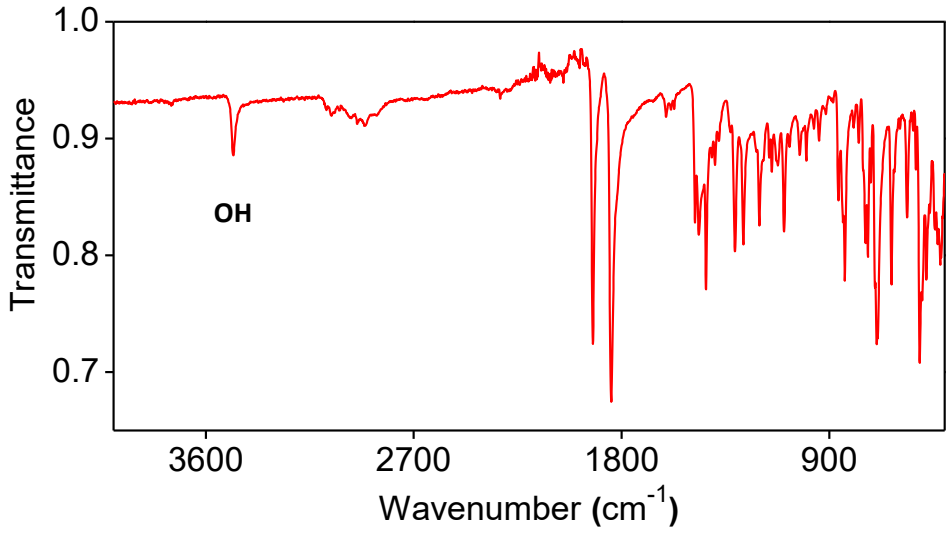


**Figure S3:** ATR-FTIR spectrum of $^{H}$**1**.

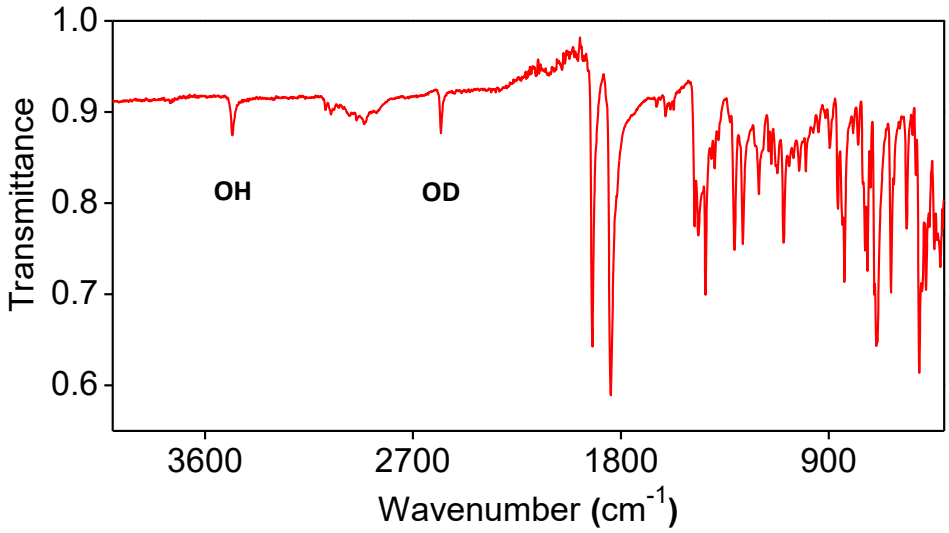


**Figure S4:** ATR-FTIR spectrum of a mixture of $^{H}$**1** and $d_1$-$^{H}$**1**.

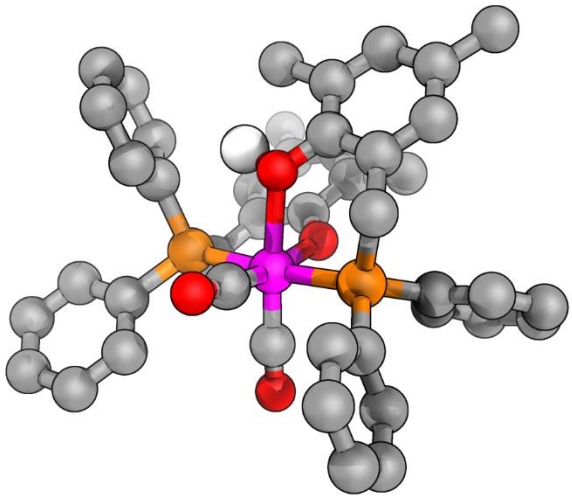

**Figure S5:** DFT computed structure of $^{H}$**1**; H-atoms attached to carbon not shown for clarity.

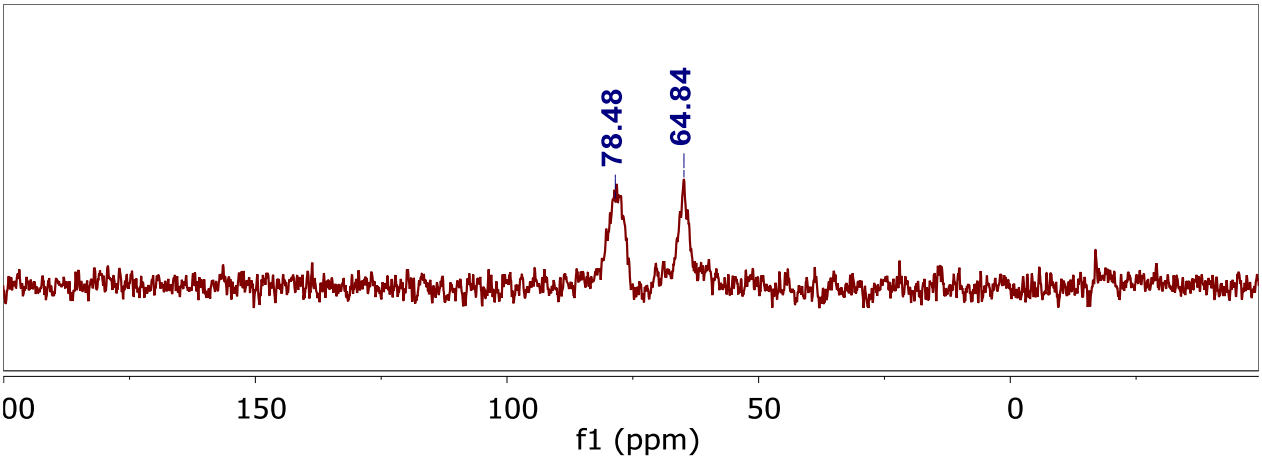


**Figure S6:** $^{31}P\{^{1}H\}$-NMR spectrum of $^{H}$**1+MeCN** in DCM.

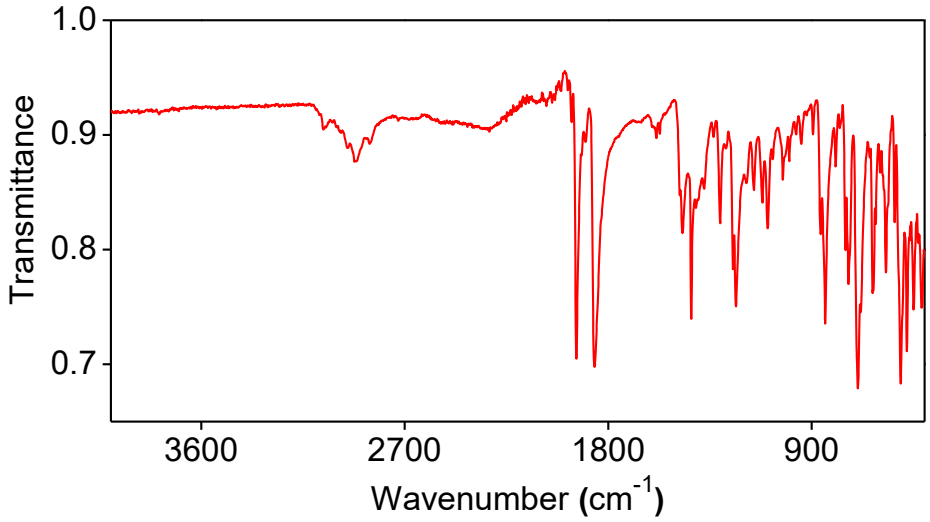


**Figure S7:** ATR-FTIR spectrum of $^{H}$**1**+**MeCN**.

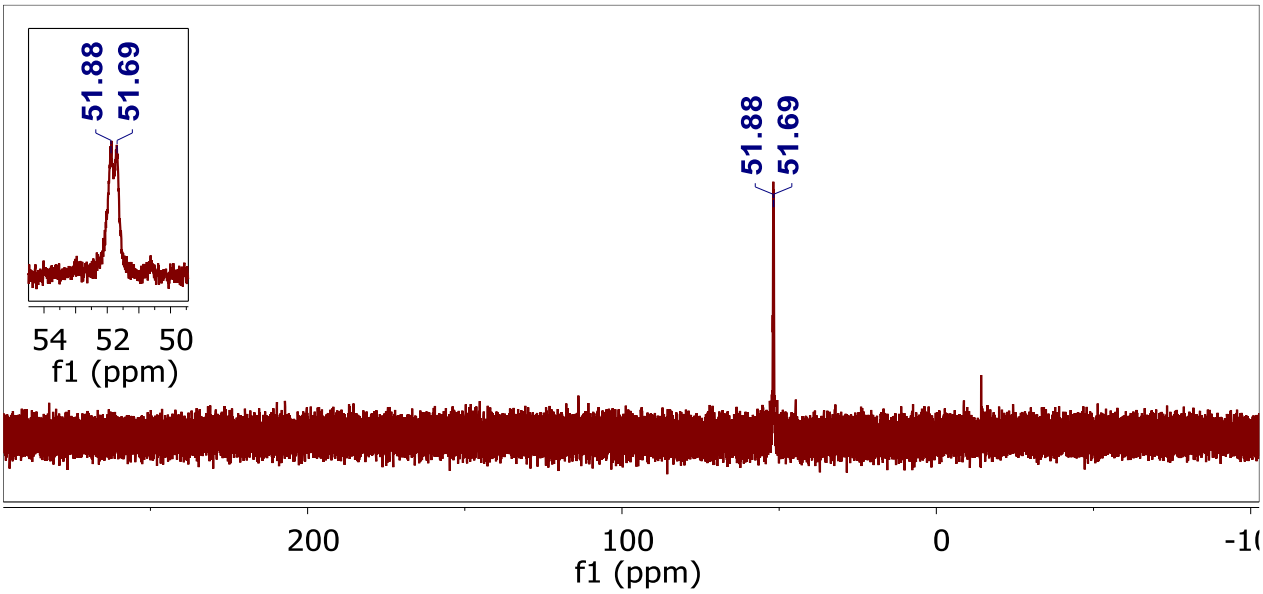


**Figure S8:** $^{31}P\{^{1}H\}$-NMR spectrum of $^{Me3Si}$**1** in hexane.

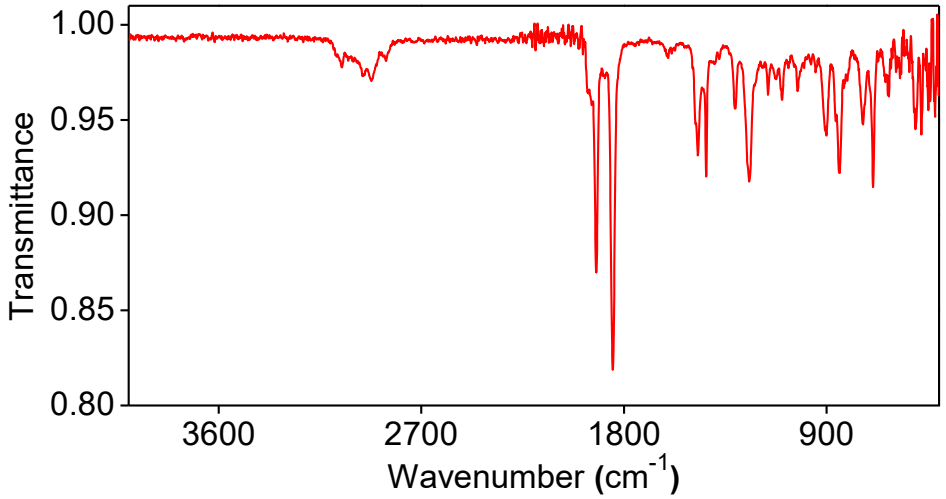


**Figure S9:** ATR-FTIR spectrum of $^{Me3Si}$**1**.

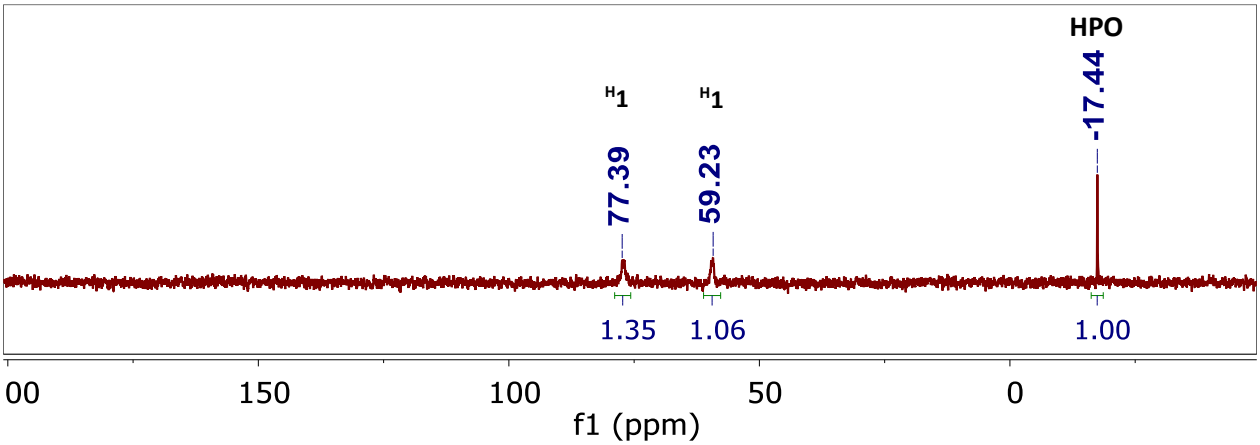


**Figure S10a:** $^{31}P\{^{1}H\}$-NMR spectrum of the reaction mixture of $^{H}$**1** + TEMPO in $d_8$-toluene.

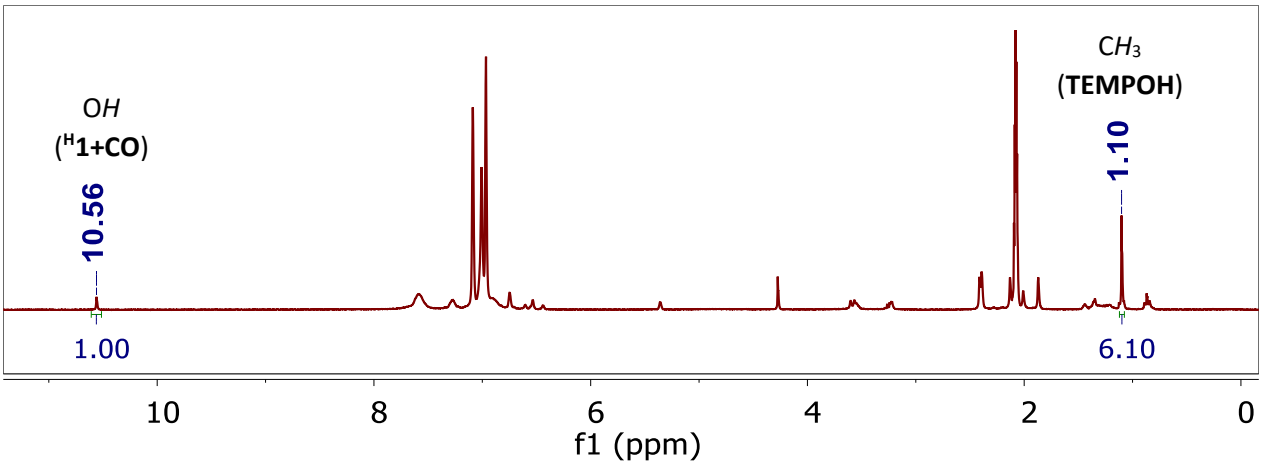


**Figure S10b:** $^{1}$H-NMR spectrum of the reaction mixture of $^{H}$**1** + TEMPO in $d_8$-toluene.

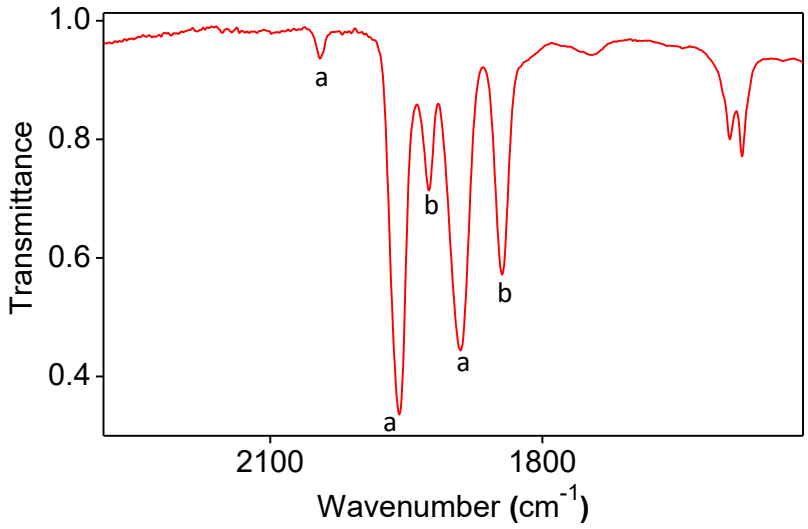


**Figure S10c:** ATR-FTIR spectrum of the reaction mixture of $^{H}$**1** + TEMPO. Peaks corresponding to $^{H}$**1+CO** is marked 'a' and the peaks corresponding to $Mn^{II}$[**1**] is marked 'b'.[1]

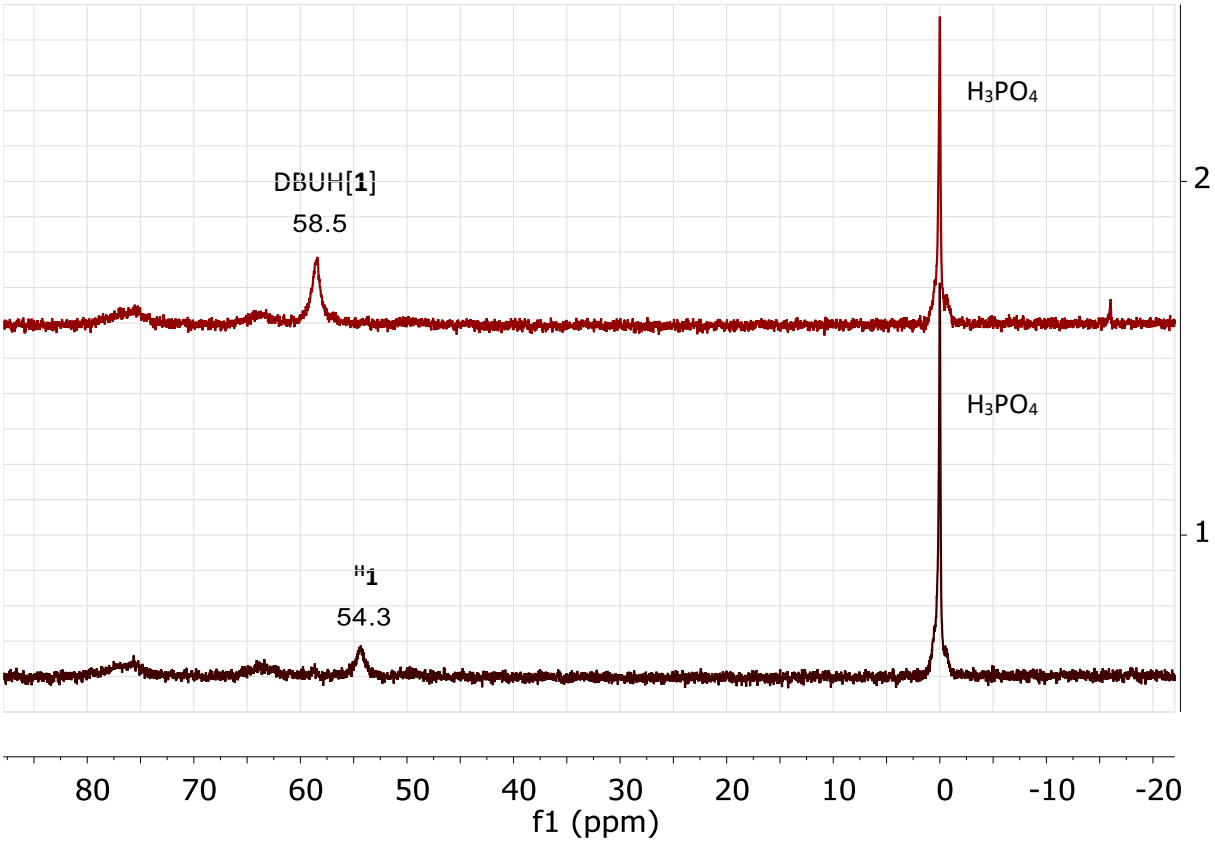


**Figure S11a:** $^{31}P\{^{1}H\}$-NMR spectrum of $^{H}$**1** (1) before and (2) after the addition of DBU in DCM, with an internal standard (capillary insert) of $H_3PO_4$ in $D_2O$.

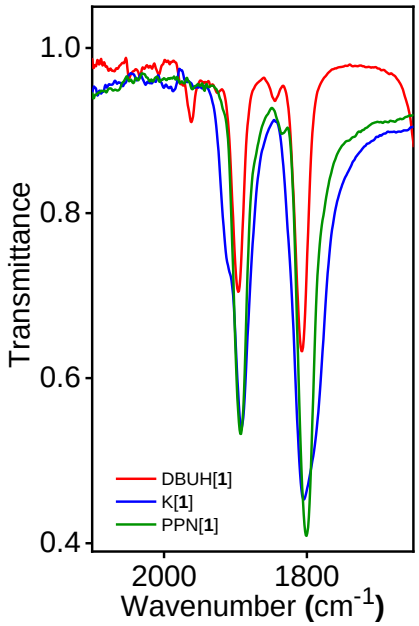


**Figure S11b:** ATR-FTIR spectra of the reaction mixture of $^{H}$**1** + DBU (red), K[**1**] (blue) and PPN[**1**] (green).

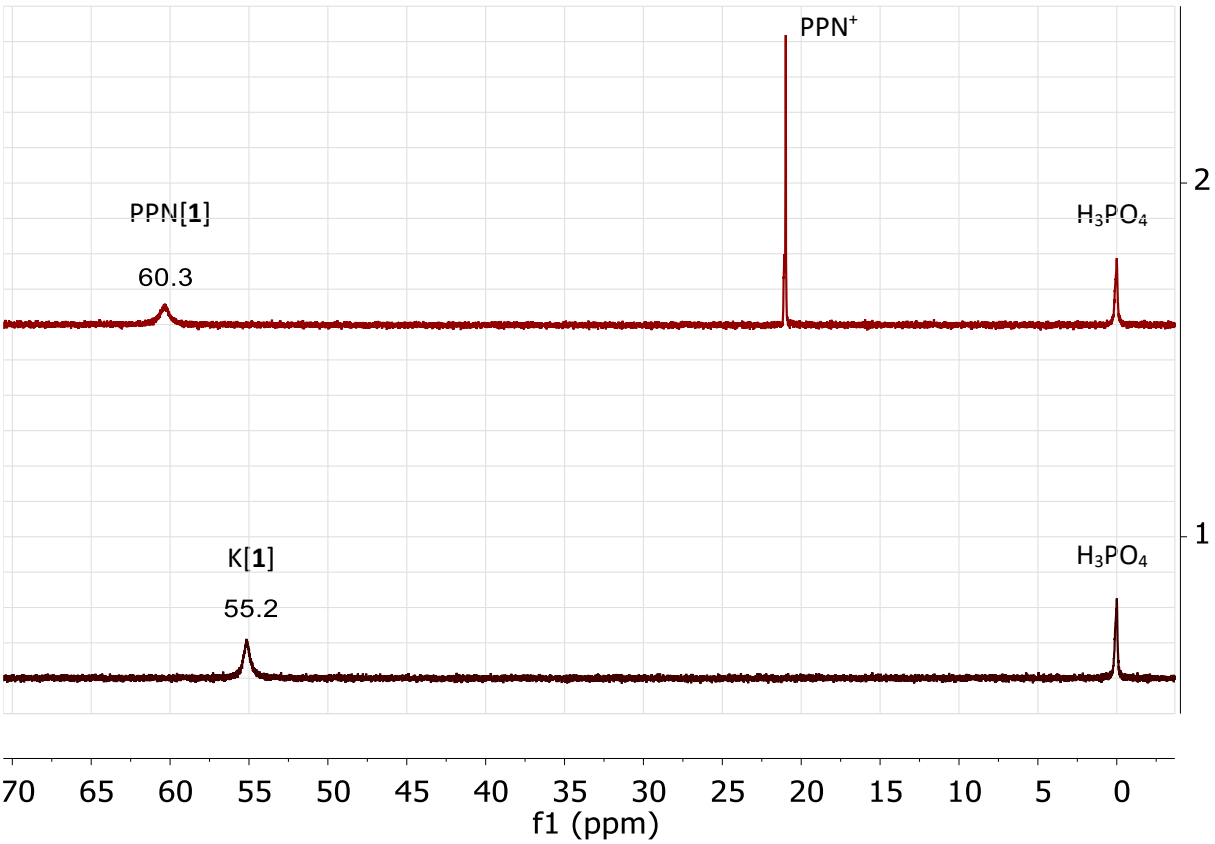


**Figure S12:** $^{31}P\{^{1}H\}$-NMR spectrum of K[**1**] (1) before and (2) after the addition of [PPN]Cl in DCM, with an internal standard (capillary insert) of $H_3PO_4$ in $D_2O$.

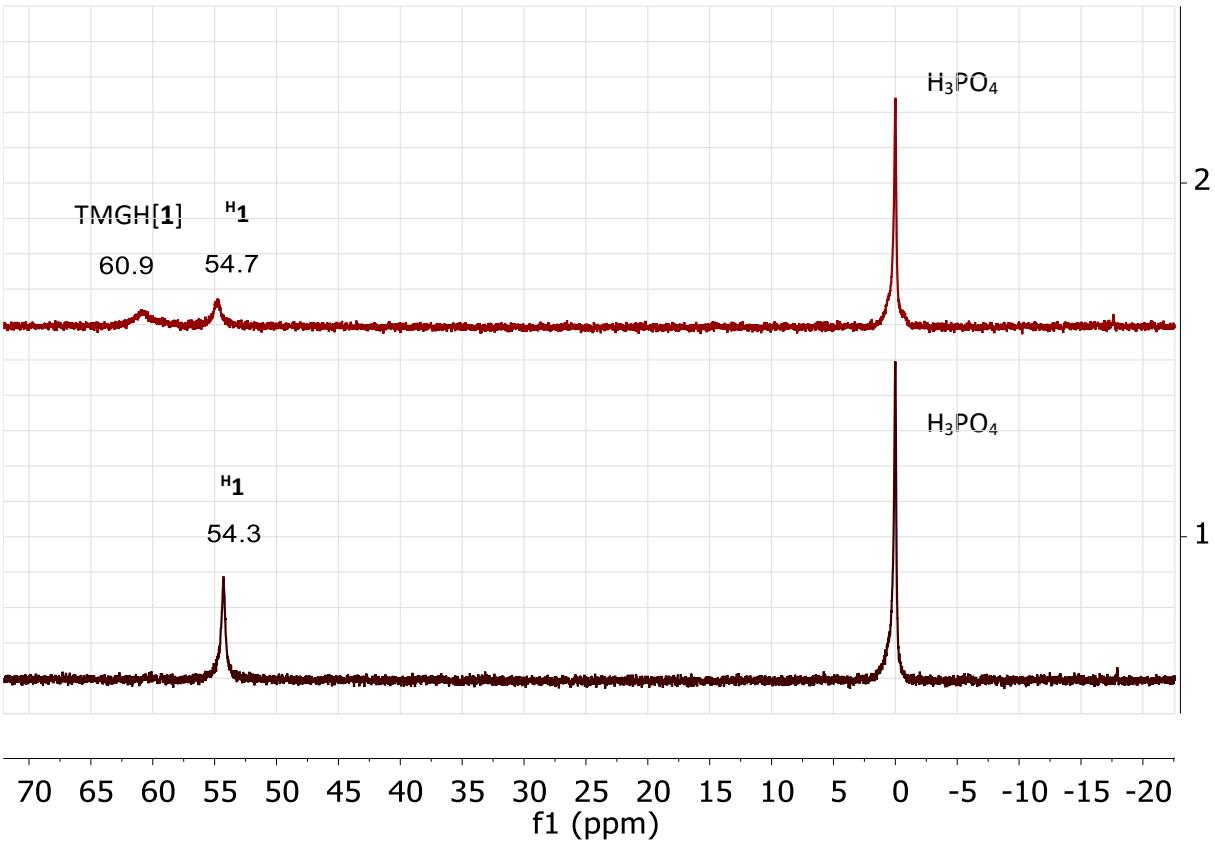


**Figure S13:** $^{31}P\{^{1}H\}$-NMR spectrum of **$^{H}$1** (1) before and (2) after the addition of TMG in DCM, with an internal standard (capillary insert) of $H_3PO_4$ in $D_2O$.

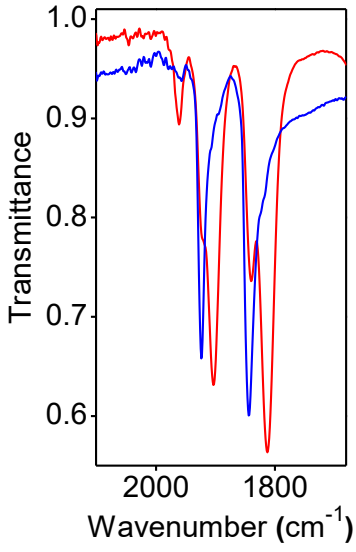


**Figure S14:** ATR-FTIR spectra of the reaction mixture of **$^{H}$1** + TMG (red) and **$^{H}$1** (blue).

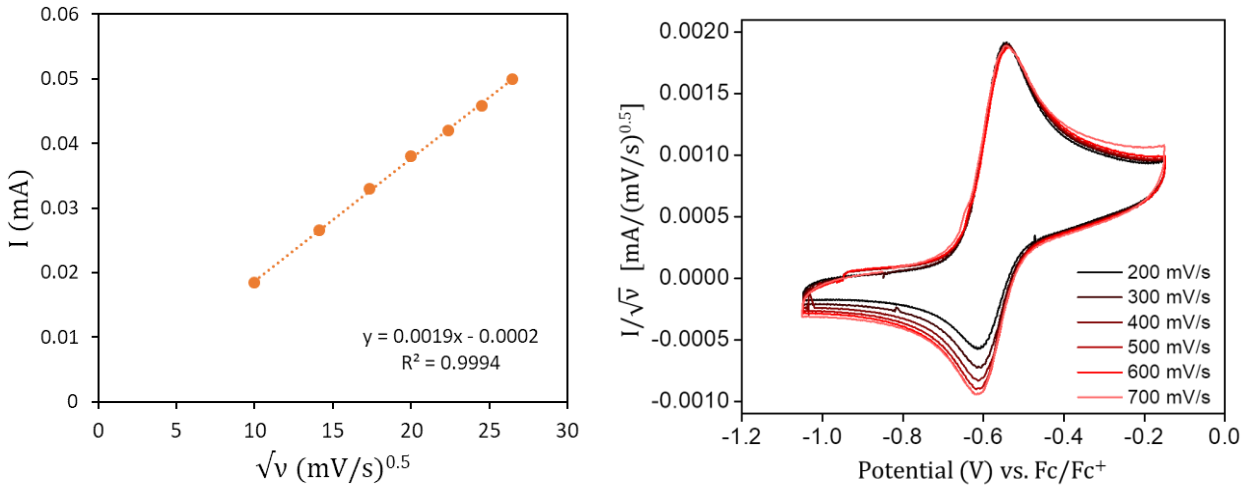


**Figure S15:** A plot of current (I) vs. square root of scan rate (ν) (left) and a plot of current/sqrt(scan rate) vs. potential (right) of 0.001 M K[**1**] in MeCN. Experimental conditions; 0.1 M $[Bu_4N][PF_6]$, glassy carbon working electrode, $Ag/AgNO_3$ reference electrode with a CoralPor™ separator, and platinum auxiliary electrode. Scan direction anodic.

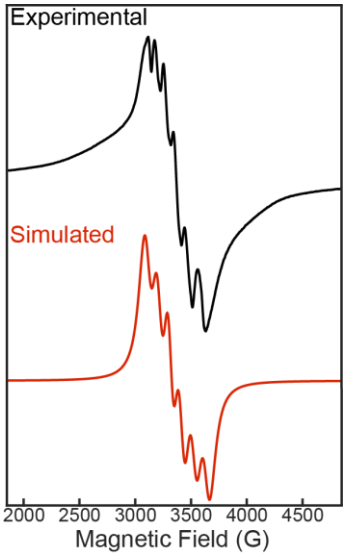


**Figure S16:** X-band EPR spectrum (77 K) of a reaction of K[**1**] with $[NO][BF_4]$.

**EPR methods:** To a solution of K[**1**] (30 mg, 0.03 mmol, 1 eq.) in 1 mL DCM was added $[NO][BF_4]$ (4 mg, 0.03 mmol, 1 eq.). The reaction was stirred vigorously for 10 min during which the solution turned green. The green solution was frozen in liquid nitrogen and an EPR spectrum was collected at 77K. The reported EPR spectrum was acquired on a Bruker EMX 390 spectrometer. Microwave frequency = 9.437 GHz, experimental range = 1850 to 4850 G, mod amp = 0.4 G, attenuation = 25 dB, scans = 12, time constant = 40. The EasySpin[2] software package was used to perform least-squares refinement of the experimental data. Simulation Parameters: spin = 5/2, nucleus = Mn, g = 1.9946, 2.0108, A = 302.7533, 0.0296 MHz, line broadening (Voigtian) = 35 MHz (Gaussian contribution) and 75 MHz (Lorentzian contribution), fitting technique: Nelder/Mead Simplex.

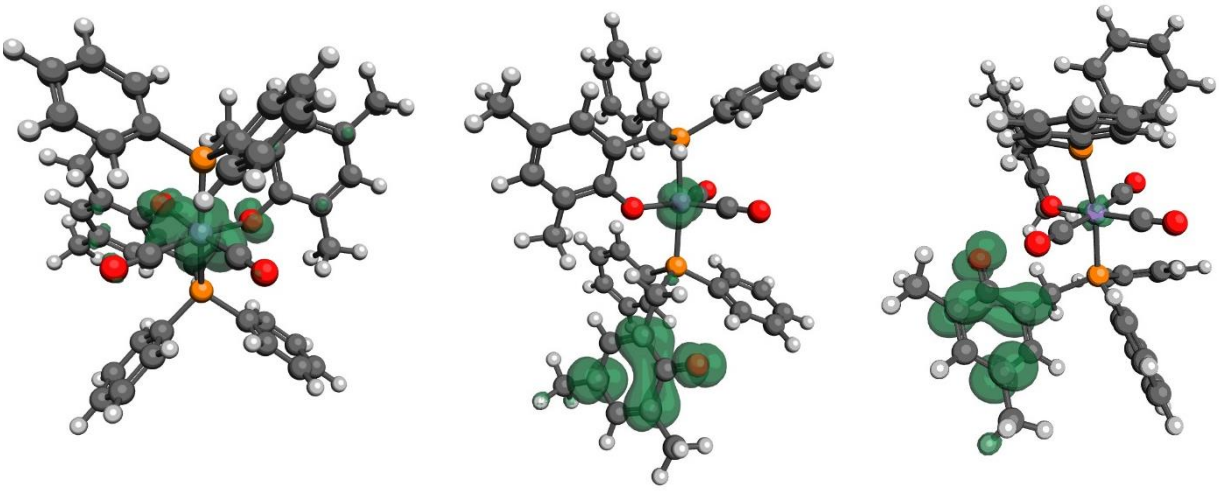

**Figure S17:** Mulliken spin density (green +/-) for the compounds $^{H}$**1**, $^{H}$**1'**, and $^{H}$**1+CO** minus a H-atom (isovalue 0.02).

**Table S1**. Mulliken spin density on selected atoms for $^{H}$**1**, $^{H}$**1'**, and $^{H}$**1+CO** minus a H-atom

| | spin density on Mn | spin density on semiquinone |
|---|---|---|
| $^{H}$**1** minus H-atom | 0.96 | 0.03 |
| $^{H}$**1'** minus H-atom | 0.03 | 0.95 |
| $^{H}$**1+CO** minus H-atom | 0.003 | 0.96 |

The spin density of the three computed doublet compounds resulting in loss of H-atom indicate a disparate metal vs. ligand radical character. The loss of an H-atom from the 18-e– isomer of $^{H}$**1** results in a metallo-radical, whereas loss of an H-atom from the 16-e– isomer $^{H}$**1'**, or the 18-e– complex $^{H}$**1+CO**, results in the formation of a ligand-based radical. Unfortunately, experimental evidence of a LS Mn(II) species to corroborate these computational findings have so far been unsuccessful.

**X-ray Crystallography**

Low-temperature X-ray diffraction data for $^{H}$**1+MeCN** (Rlacy29) and $^{H}$**1** (Rlacy36) were collected on a Rigaku XtaLAB Synergy diffractometer coupled to a Rigaku Hypix detector with Cu Kα radiation (λ = 1.54184 Å), from a PhotonJet micro-focus X-ray source at 100 K and 253K, respectively. The diffraction images were processed and scaled using the CrysAlisPro software.[3] The structures were solved through intrinsic phasing using SHELXT[4] and refined against $F^2$ on all data by full-matrix least squares with SHELXL[5] following established refinement strategies.[6] All non-hydrogen atoms were refined anisotropically. All hydrogen atoms bound to carbon were included in the model at geometrically calculated positions and refined using a riding model. Hydrogen atoms bound to oxygen were located in the difference Fourier synthesis and subsequently refined semi-freely with the help of distance restraints. The isotropic displacement parameters of all hydrogen atoms were fixed to 1.2 times the Ueq value of the atoms they are linked to (1.5 times for methyl groups). $^{H}$**1+MeCN** (Rlacy29) contains disordered solvent molecules of $CH_2Cl_2$ that were included in the unit cell but could not be satisfactorily modeled. Therefore, those solvents were treated as diffuse contributions to the overall scattering without specific atom positions using the solvent mask routine in Olex2.[7]


1. Kadassery, K. J.; MacMillan, S. N.; Lacy, D. C., Resurgence of Organomanganese(I) Chemistry. Bidentate Manganese(I) Phosphine–Phenol(ate) Complexes. *Inorg. Chem.* **2019,** *58* (16), 10527-10535.
2. Stoll, S.; Schweiger, A., *Journal of Magnetic Resonance* **2006,** *178*, 42-55.
3. *CrysAlisPro*; Rigaku OD, The Woodlands, TX, 2015.

4. Sheldrick, G. M., SHELXT – Integrated Space-Group and Crystal-Structure Determination, *Acta Cryst.*, **2015**, *A71*, 3-8.
5. Sheldrick, G.M., A Short History of SHELX, *Acta Cryst*., **2008**, *A64*, 112-122.
6. Müller, P., Practical Suggestions for Better Crystal Structures, *Crystallogr. Rev.*, **2009**, *15*, 57-83.
7. Dolomanov, O.V.; Bourhis, L.J.; Gildea, R.J.; Howard, J.A.K.; Puschmann, H., OLEX2: A Complete Structure Solution, Refinement and Analysis Program, *J. Appl. Cryst.*, **2009**, *42*, 339-341.